13th International Symposium on Particle Image Velocimetry – ISPIV 2019
Munich, Germany, July 22-24, 2019

Effect of the pore geometry on pressure distribution within a bubble penetrating a single pore

Shadi Ansari and David S. Nobes*

University of Alberta, Department of Mechanical Engineering, Edmonton, Canada

* david.nobes@ualberta.ca

Abstract

The mobility of multi-phase flow passing through a porous media can be modeled using the pressure distribution within the phases. In addition to velocity, viscosity and interfacial properties of the phases, the pore space geometry has a significant effect on pressure distribution of the discrete phase. The aim of this study has therefore been to establish a fundamental understanding of effect of the surface roughness and shape of the pore on pressure distribution within the phases. In order to achieve this goal, an isolated bubble flow passing two different pore geometry shapes with the same aperture size, with one having a different pore surface roughness, were studied. The velocity distribution and the deformation of the dispersed phase in pore space was evaluated using a particle shadowgraph velocimetry (PSV) experimental setup. Observation of the bubble shape shows that there was a significant difference in the deformation of the bubble as it passes the different pore geometries. A similar trend of flow motion of the dispersed phase entering the pore space was observed in all cases. As the phase exits the pore, however, different flow motion and pressure distribution was observed within the dispersed phase. Pinning of the bubble was more significant for the pore with higher surface roughness resulting in a higher-pressure variation within the phase. This work contributes to existing knowledge multi-phase flow thorough porous media by accounting for geometry and surface properties of the pore space.

1 Introduction

Flow in different industrial application such as oil recovery (Huang & Varadaraj, 1996), food processing (Soottitantawat et al., 2005) and macromolecular delivery (Nakano, 2000) are mainly present in the form of a multi-phase flows. The results of studies on multi-phase flows passing through confined geometries indicates that the flow of dispersed phase larger than the length scale of the flow passage has higher resistance as compared to a single phase flow (Ezeuko, Wang, & Gates, 2012). The resistance is introduced due to the deformation of the dispersed phase which arises from the interfacial interaction between the phases and the flow passage (Smith & Crane, 1930). Experimental and the numerical studies have shown that the flow of a multi-phase fluid through rectangular channels is affected by the viscosity and the interfacial properties of fluid as well as the geometrical properties of flow passage (Jin, Kim, Lee, & Yoo, 2010; Soltani, Sabbagh, & Nobes, 2018). The effect of these properties on the flow characteristics becomes more significant as the flow passes through a confined geometry with varying cross sections such as pore space.

The interaction of the multi-phase flow through a pore can be studied by determining pressure distribution as a representative parameter for the flow properties. The pressure in this condition can be calculated using an indirect method proposed in our previous studies (Ansari, Yusuf, et al., 2018; Ansari, Sabbagh, Soltani, & Nobes, 2018). In this method, pressure variation of the dispersed phase is determined based on the deformation of the phase and pressure in the continuous phase is calculated by applying Navier-Stokes on the velocity distribution. Shape analysis and the velocity measurement is achieved using optical diagnostic techniques such as micro particle shadow velocimetry (μ-PSV). The optical measurement provides more detailed results required for the shape deformation and the velocity distribution with respect to time and position.

The main objective of this study is to investigate the effect of shape and roughness of the pore space on pressure distribution within the multi-phase flow. In order to achieve this goal, an isolated bubble will be considered as a dispersed phase to pass through pore space and the deformation and velocity will be monitored using PIV. The results of this study will aim to provide better understanding of the effect of pore surface properties on pore scale capillary pressure and fluid motion within a porous media.

2 Theory

An example of the shape analysis of different stages of bubble deformation passing through a pore is shown in Figure 1(a)(Ansari, Sabbagh, et al., 2018). Based on the theory introduced by Jamin (1860), the pressure change within the dispersed phase (Δp^*) is inversely proportional to the change in the radii of curvature of the trailing (R_T) and leading edge(R_L) and can be written as:

$$\Delta p^* = \gamma_{cd}\left(\frac{1}{R_\mathrm{L}} - \frac{1}{R_\mathrm{T}}\right) \tag{1}$$

Depending on the location of dispersed phase from the pore throat, deformation of the dispersed will result in different pressure distribution as shown in Figure 1(b). The trend of the pressure change calculated from the shape analysis is similar to the one proposed by the theory. The results of the previous studies, however, highlighted the potential effect of different parameters such as interfacial properties of the wall of the flow passage and the geometrical shape of the pore on the magnitude and the trend of the change in the pressure distribution within the phases. The pressure in these conditions are difficult to model and simulate using numerical approaches. Therefore, pressure is needed to be calculated experimentally using the optical diagnostic techniques where there is no need to apply the BC's such as wall interfacial characteristics to determine the pressure distribution.

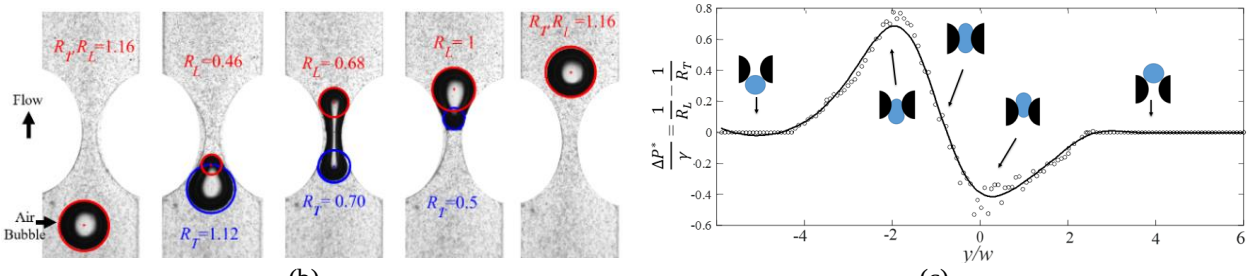

(b) (c)

Figure 1 : An example of determining pressure from (a)raw images with fitted radii of curvatures and (b)pressure variation with respect to position along a pore throat(Ansari, Sabbagh, et al., 2018)

3 Experimental Setup and Image processing

The PSV experimental setup used to evaluate flow motion of a bubble in different pore geometries is shown in Figure 2(a). A camera (4M180, IO Industries Inc.) operating at 50 Hz of frame rate coupled with the 110 mm lens is used to focus the central plane of a flow channel. The system is back-illuminated using 4×4 high current LED (BX0404-520 nm; Advanced Illumination Inc.) operating in a continuous mode. To study the effect of the pore interface on the pressure distribution, three different main channels were designed in this experiment as shown in Figure 2(b). The flow cell is made of two layers of a main flow channel and an optical window access. These flow channels contain different pore geometry shapes with the same aperture size (w) shown in the detailed view of (I) and (II) of the Figure 2(b). The effect of the roughness on the pressure is also studied by changing the pattern of the wall of the pore as shown in Figure 2(III) and (IV).

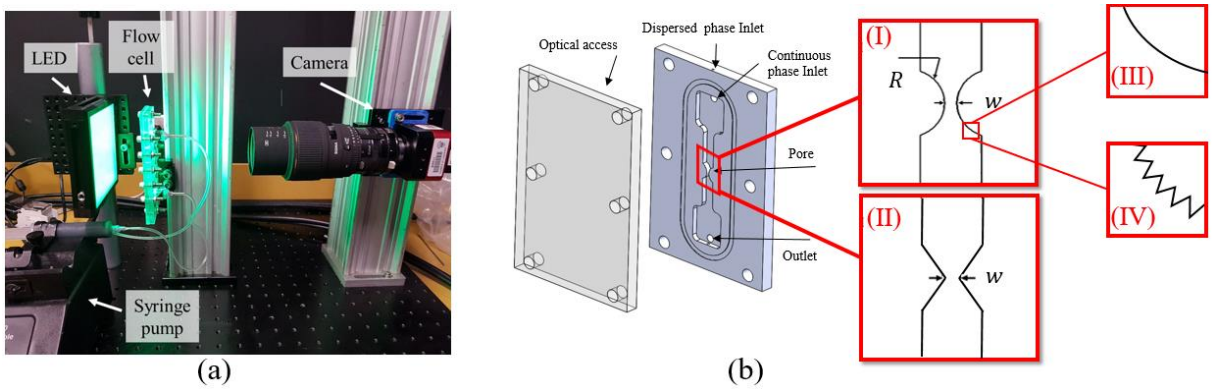

Figure 2: Annotated image of (a) the μ-PIV setup and (b) the flow cell with geometry to be used in experiments.

The designed flow channels are manufactured from photo reactive resin material using the stereolithography (SLA) additive manufacturing technique (Form 2, Formlabs Inc. USA). A comparison between the design and a picture of manufactured flow cells are shown in Figure 3. As it can be seen in the figure the flow cell was designed to have 1 mm for pore space and after the manufacturing the pore spaces are 1.04, 1.05 and 1 mm for smooth, rough and sharp pore, respectively. The roughness of the pore shown in Figure 3(a) is ~0.17 mm for each feature designed on the surface of the pore. The flow cells are symmetric for all cases as indicated by the radius of the pillar representing the pore space.

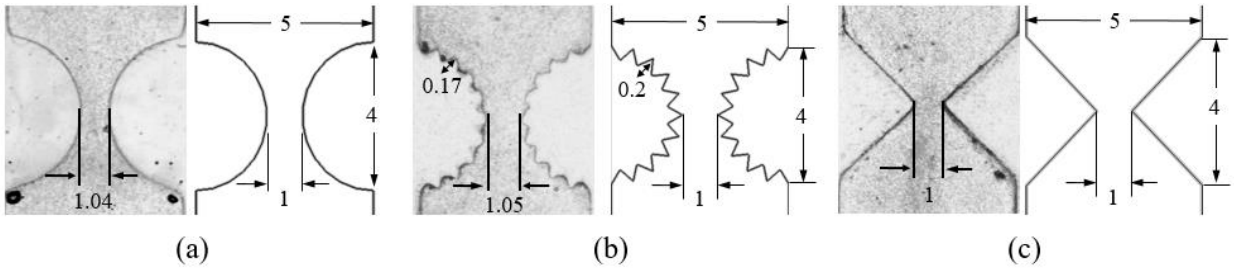

Figure 3: A picture and schematic of manufactured flow cells (a) smooth round pore, (b) rough round pore and (c) sharp pore (all dimensions are in mm)

In all of the experiments, 100% pure glycerol (Glycerol-Molecular Biology; Fisher BioReagents™, USA) with density of 1.261 g/cm^3 and viscosity of 1.412 Pa.s is used as the continuous phase. An isolated air bubble was used as the dispersed phase passing through the pore space. The dispersed phase was introduced using an inlet designed at the bottom of the channel at constant time intervals. In order to track the motion and deformation of the bubble, images were pre-processed as shown in Figure 4. As it can be seen in the raw image, Figure 4(a), the air bubble in this study was captured with a bright region in the center of the bubble shadow arising from the diffraction of light as a result of air having a different refractive index to the glycerol. Due to the density difference of the phases, the bubble moves from bottom to top of the channel in the opposite direction to the gravity vector. The continuous phase was also injected at 0.2 ml/min using a syringe pump (PHD 2000, Harvard Apparatus) in the same direction of the bubble's motion.

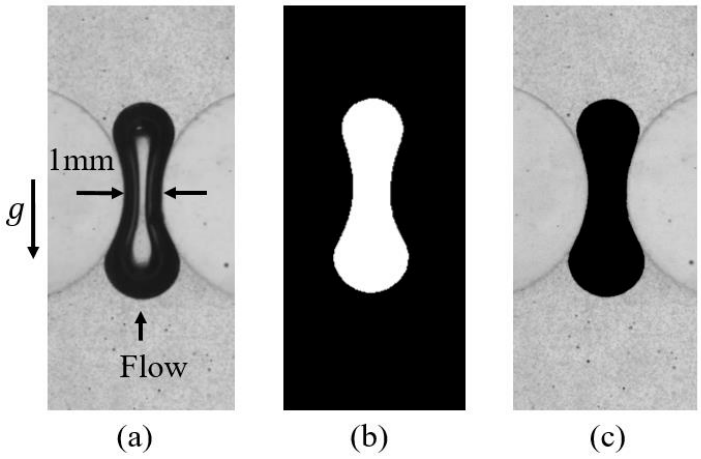

Figure 4: Image pre-processing sample (a) raw picture of bubble passing through a pore space, (b) masked dispersed phase and (c) masked continuous phase

The first step of the image pre-processing was to isolate the dispersed phase. This can be achieved using the intensity difference between the dispersed phase and continuous phase in the field. The picture of the detected dispersed phase was determined using an edge recognition (function *edge*; Matlab2018a, The MathWorks, Inc.) approach as shown in Figure 4(b). By masking the detected dispersed phase region from the raw image, the isolated continuous phase can be determined as shown in Figure 3(c). The isolated dispersed phase can be further used to evaluate the pressure change in the phase. Having the outer region of the phase, the radius of the curvature of the leading and trailing edge can be estimated and the pressure can be calculated using eq. (1) for each location where the bubble passes the pore space.

4 Results

Pictures of an isolated bubble passing through the different pore geometries with respect to time are presented in Figure 5. Shown in location (a) for all pore geometries, the bubble has a similar size and symmetric shape before it enters the pore space. The bubble has a slightly oval shape due to the presence of the confining, converging wall of each channel. As the bubble approaches the pore space, indicated in location (b), the bubble begins to deform significantly to enable the flow passage. In this condition, the bubble has a smaller radius leading edge compared to its trailing edge. The leading edge of the bubble decreases to its minimum value when the bubble's interface aligns with the pore throat shown in Figure 5(c). The same trend of change in the leading edge was observed for the bubble entering the pore for all shapes three channel shapes.

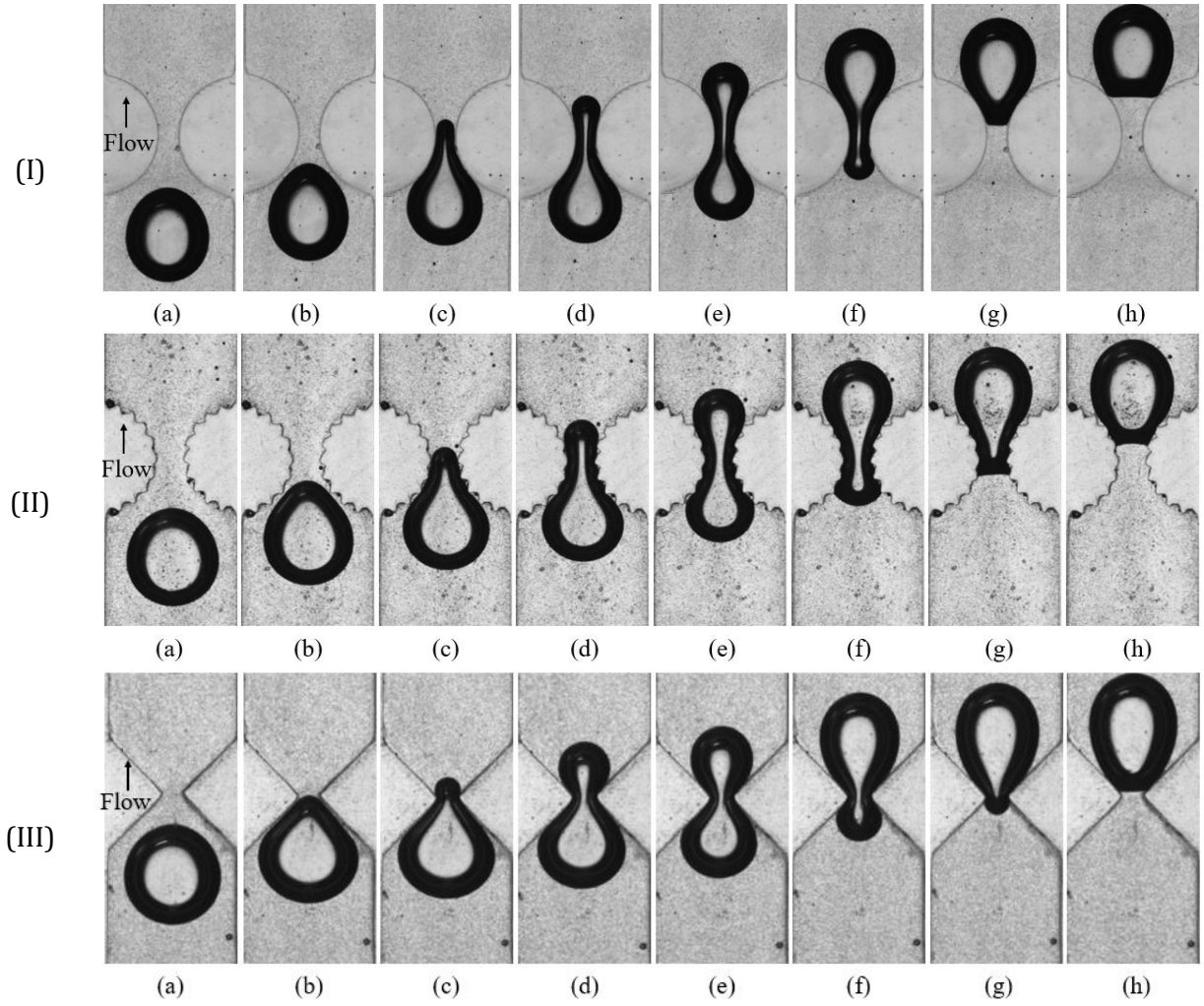

Figure 5: Bubble passing through (I) round pore (II) round pore with rough surface and (III) pore with sharp corner

As the bubble's front edge passes the pore throat, the leading edge radius increases and the trailing edge radius starts to decease. The change in the radius of the trailing edge, however, is highly affected by the geometrical properties of the pore space. It can be seen in Figure 5 that there is a significant difference between the motions of bubble exiting the pore space for different pore geometries. The

differences can be clearly observed in location (g) of Figure 5. For the case of the smooth pore, the bubble has a convex interfaces as it exits the pore throat. Shown in location (h), the trailing edge of the bubble becomes flat at the point when the bubble is about to detach from the pore. This is due to the presence of the bulk flow motion of the continuous phase in the pore space and the pinning of the bubble to the solid surface.

The pinning effect is more significant in the case of the round pore with surface roughness as shown in Figure 5(II). It can be seen that the contact point between the bubble and pore solid interface for the upper portion of the bubble, represented in (c) to (h), is only at the peak of the roughness pattern. For the lower part of the bubble, however, the bubble deforms to fill the geometry of the roughness. The larger contact area between the bubble and the pore space in the lower portion of the bubble results in a more significant pinning effect as shown in location (g). Figure 6 demonstrates the detail view of different exiting stages of the bubble passing through a pore with a rough surface. Shown in Figure 6(a), the bubble's lower portion fills the roughness and has similar shape as the roughness of the surface. For the locations where the trailing edge has a lower elevation than the peak of the roughness, Figure 6(a) and (c), the trailing edge has a convex shape. As the interface moves further into the pore, shown in Figure 6(b), the bubble's trailing edge transitions to a concave shape. This is due to interface pinning that occurs at the peak of the roughness. This trend of the change in the curvature of the bubble can be seen to occur for each roughness peak of the pore.

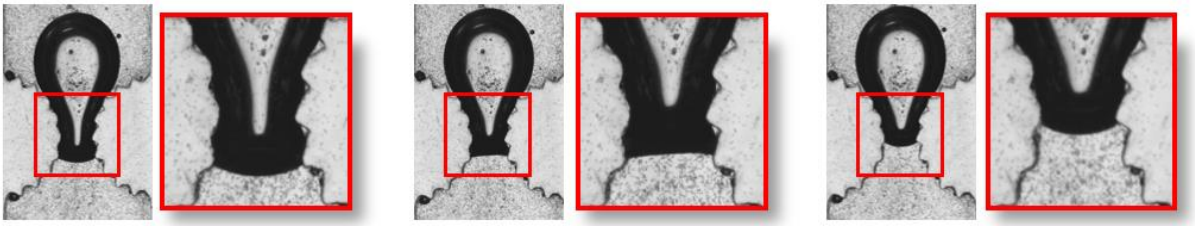

Figure 6: Pinning of a bubble at different stages exiting the pore space with rough surface

The change in the radius of curvature of the bubble at different locations corresponds to a different pressure distribution within the phase. Using the approach discussed in experimental section, the change in the radius of curvature for the bubble at different locations from the pore throat was determined and plotted in Figure 7(a). To have a better comparison of the cases, the radius of curvature (R) for each case were normalized based on the equivalent radius of the bubble (R_b) in its spherical shape and represented as R^*. The location (y) of the bubble is also normalized using the pore throat size (w) and it is offsets to align the origin with the pore throat and indicated as y^*. With the availability of a high number of data points, the change in the curvature, pressure and velocity are shown as a continuous lines in the graphs.

Shown in in Figure 7(a), for all pore space geometries, the bubble has the same radius of curvature for the leading and trailing edge before ($y^* \gtrsim -3$). This location represents the condition where bubble has spherical shape before entering the pore space. As the bubble approaches the pore throat, in the range $-3 < y^* < -2$ the radius of the leading edge decreases for all cases due to the influence of the change in the cross-sectional area of the pore space. The change in the radius of curvature for

the round pore with and without roughness follow the similar trend. Whereas, in for case of sharp pore, the radius of curvature of the leading edge occurs further downstream ($y^* \leq -1$). This is due difference in rate of change in the available area for flow passage in the different shapes of pore. The radius of curvature of the bubble's leading edge continuous to decrease and it reaches its minimum where it is aligned with the pore throat. The minimum for the leading edge occurs at $y^* \sim -1.6$ for rough and round pore and $y^* \sim -1.2$ for the sharp pore. After these locations, the radius of the leading edge increases and it reaches unity in each case where the bubble exits the pore space.

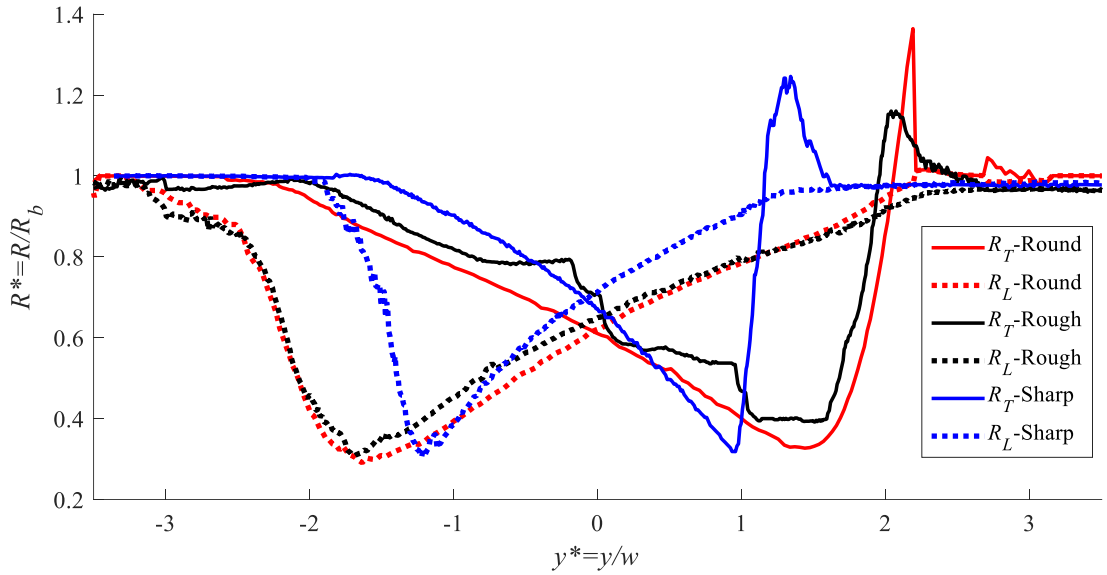

(a)

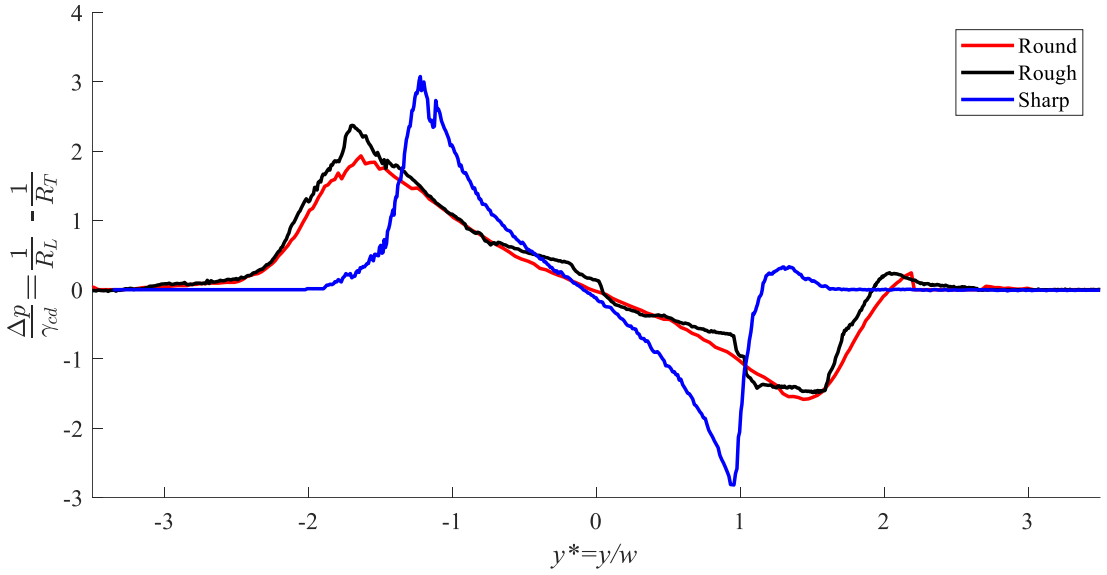

(b)

Figure 7: Plots of (a) change in the radii of curvature of leading and trailing edge of bubble passing through various pore geometries and (b) the change in the pressure of the leading and trailing edge at different locations. Leading edge: dotted line. Trailing edge: solid line.

The change in the radius of the trailing edge of the bubble showed a significant difference. Shown in Figure 7(a), the bubble has a smooth transition for the change of its radius of curvature as it enters the smooth pore throat. The radius decreases as the bubble enters the pore and it will have its minimum value when the bubbles trailing face is aligned with the pore throat ($y^* \sim 1.4$). The radius increases as the trailing edge passes the pore throat. It reaches a maximum value as it passes out of the pore space ($y^* \sim 2.2$) due to the pinning effect shown Figure 5 (h). In this condition the leading edge has a radius of curvature similar to its spherical shape whereas, the trailing edge has an almost flat surface. In the case of the roughed surface, it can be seen that the change in the radius has a stepwise trend. These steps are due to the pinning effect that occurs at each peak of the surface roughness. This phenomena was explained in detail in Figure 6. The location where the bubble reaches its minimum and the maximum trailing radius are the same as the round pore space. A similar trend is also observed for the case of the sharp pore. In this case however, the rate is different from the round pore. The change in the radius starts further upstream ($y^* \sim 0.9$) and it reaches its maximum value closer to the pore throat ($y^* \sim 1.3$).

Using the eq. (1) and the calculated radius of curvature of the trailing and leading edge shown in Figure 7(a), the change in pressure across the bubble was calculated and plotted in Figure 7(b). The bubble passing through a round pore showed a similar trend as found in our previous study (Ansari, Sabbagh, et al., 2018). For the pore with the rough surface, slightly higher pressure variation was observed in the bubble and it also shows a stepwise change in the pressure due to the pinning effect. The pressure change in the sharp pore space showed a more significant change compared to the others. This arises due to the more variation in the radius of curvature of the leading and trailing edge of bubble in this case.

The change in the pressure will lead to different velocity variation of the bubble as it passes through the pore. The velocity of the bubble for the different pore shapes is plotted in Figure 8. It can be seen that the bubble decelerates as it enters the pore area due to the negative pressure distribution within the phase. As the leading edge of the bubble passes the pore, the bubble accelerates. In the case of the round pore, it reaches a value higher than its initial velocity before it approaches the pore. This is due to the decrease in the available cross-sectional area for the flow. For the rough and sharp pore shapes however, the velocity doesn't reach its initial value. This variation is because of the higher pressure change introduced to the bubble results in more resistance for the flow passage and the pinning effect that occurs in the solid interface. As the bubble exits the pore space, the velocity decreases again because of the pinning phenomena observed in location (h) of Figure 5(I), (II) and (III). It can be seen that the bubble accelerates more as it passes through the smoother surface. The increase in velocity is not that significant for the rough shape pore due to the presence of the pining of the bubble at each peak of the pore roughness. This phenomena emphasizes the importance of the pore geometry on the motion and deformation of bubble.

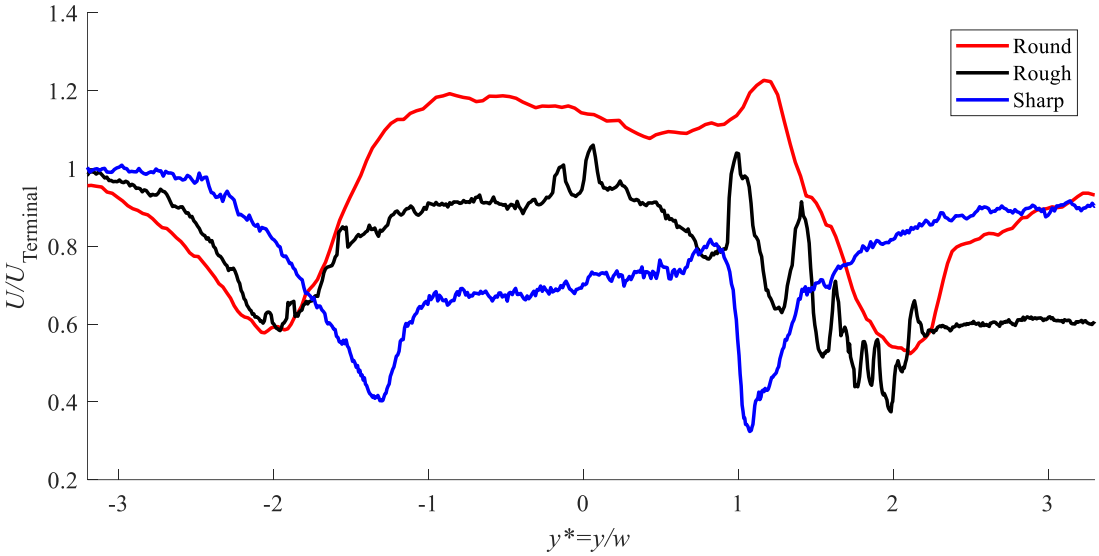

Figure 8:change in the velocity of bubble passing through the pore space

5 Conclusion

The effect of pore geometry on the deformation, pressure and velocity of an isolated bubble passing through a pore was studied using PSV. Three different pore spaces of round, rough and sharp pore were considered for this study. The results indicated that the radius of curvature for the leading and trailing edges of the bubble passing through a pore space is highly affected by the geometry of the pore solid interface. In the case of the round and sharp pore space, a smooth transition in the radius of curvature of leading and trailing edge were observed. For the rough interface, however, a step change was show for the trailing edge due to the pinning effect. The change in the radius of curvature of the faces corresponds to the variation in the pressure field at different in the pore. The pressure distribution ultimately resulted in a variation in the velocity of the bubble passing through the pore. A higher velocity decrease was observed for the sharp pore due to the more significant change in the flow passage geometry. The roughness of the surface also had an effect on the deceleration of the bubble. The results confirmed that the Jamin effect is highly affected by the pore space geometry and the surface roughness. This study offers some important insights regarding the effect of pore shape on the mobility of multiphase flow through porous region.

Acknowledgements

The authors gratefully acknowledge financial support from Natural Sciences and Engineering Research Council (NSERC) of Canada, the Alberta Ingenuity Fund, the Canadian Foundation for Innovation (CFI) and RGL Reservoir Management Inc. Special thanks to Tod Vandenberg for his help.

References

Ansari S, Sabbagh R, Soltani H, and Nobes DS (2018) Flow visualization of a bubble penetration through porous media in SAGD process using μSPIV. In *5th International Conference on Experimental Fluid Mechanics – ICEFM 2018 Munich*

Ansari S, Yusuf Y, Sabbagh R, Soltani H, Kinsale L, and Nobes DS (2018) An imaging derivation of the pressure field of a multi-phase flow in a porous media using μ-SPIV. *19th International Symposium on the Application of Laser and Imaging Techniques to Fluid Mechanics・Lisbon, July16-19, 2018*.

Ezeuko C, Wang J, and Gates I (2012) Investigation of Emulsion Flow in SAGD and ES-SAGD. *Proceedings of SPE Heavy Oil Conference Canada* 1–16.

Huang JS, and Varadaraj R (1996) Colloid and interface science in the oil industry. *Current Opinion in Colloid & Interface Science* 1:535–539.

Jamin MJ (1860) Memoire sur l'equilibre et les mouvements de liquides dans corps poreux. *Compt. Rend. Acad. Sci.* 50:172–176.

Jin BJ, Kim YW, Lee Y, and Yoo JY (2010) Droplet merging in a straight microchannel using droplet size or viscosity difference. *Journal of Micromechanics and Microengineering*.

Nakano M (2000) Places of emulsions in drug delivery. *Advanced Drug Delivery Reviews* 45:1–4.

Smith WO, and Crane MD (1930) The jamin effect in cylindrical tubes. *Journal of the American Chemical Society* 52:1345–1349.

Soltani H, Sabbagh R, and Nobes DS (2018) The passage of bubbles rising through a confining rectangular geometry. *Physics of Fluids* 10:103302.

Soottitantawat A, Bigeard F, Yoshii H, Furuta T, Ohkawara M, and Linko P (2005) Influence of emulsion and powder size on the stability of encapsulated D-limonene by spray drying. *Innovative Food Science and Emerging Technologies* 6:107–114.